



OPEN

Activated vitamin D₃ improves the microbiota and intestinal barrier in type 2 diabetic mice via modulating AMPK activation

Lewen Zhang^{1,2,4}, Lijuan Zhao^{1,4}, Yudie Hu¹, Min Xiao¹, Yuxuan Zheng¹, Xun Wei³, Chunlan Xiao¹✉ & Zhengyu Zhou¹✉

The association between vitamin D and type 2 diabetes mellitus (T2DM) pathogenesis, particularly through gut microbial interactions, requires further elucidation. This study investigates vitamin D-microbial interactions in T2DM pathogenesis, targeting their modulation of inflammatory cascades and redox imbalance. After successfully establishing a T2DM mouse model using a high-fat diet (HFD)/streptozotocin (STZ), the mice were treated with activated Vitamin D₃ (1,25(OH)₂D₃) for 4 weeks. Systemic parameters including glycemic control (FBG, GHbA1c, insulin), oxidative stress biomarkers (ROS, MDA, T-AOC, CAT), proinflammatory cytokines (TNF- α , TNF- β), and lipopolysaccharide (LPS) levels were measured. Microbial community profiling via 16 S rRNA sequencing, while colonic redox status (MDA/SOD), barrier integrity (ZO-1/Occludin), and metabolic signaling (SIRT1, p-AMPK) were analyzed. T2DM mice exhibited gut microbial dysbiosis, marked by significant enrichment of *Enterococcus* and *Enterobacter*, whose abundances correlated positively with hyperglycemia, inflammation, and oxidative stress. Histopathological analyses concurrently demonstrated compromised intestinal barrier integrity, characterized by reduced ZO-1/Occludin protein expression and SOD activity. Notably, treatment with 1,25(OH)₂D₃ effectively mitigated these pathological changes and concurrently enhanced AMPK phosphorylation in the colon. These findings position vitamin D-AMPK axis modulation as a promising therapeutic strategy for microbiota-metabolism crosstalk in T2DM, highlighting its translational potential for clinical validation.

Keywords T2DM, Intestinal microbiota, 1,25(OH)₂D₃, Oxidative stress, Inflammation

Diabetes is a systemic, progressive disease with considerable phenotypic heterogeneity, posing a major public health challenge in the 21st century¹. Type 2 diabetes mellitus (T2DM) is the most prevalent form of diabetes, accounting for 90% of all cases, and is characterized by chronic low-grade inflammation and chronic activation of the immune system². Although its etiology is complex, epidemiological studies have established that genetic predisposition, dietary habits, obesity, and deficiencies in vitamins D and K are more common in T2DM patients, positioning them as viable therapeutic targets for disease management³. Recent evidence suggests that intestinal metagenomes also drive T2DM development by interacting with the environment to participate in host physiological maintenance^{3,4}.

The collective community of bacteria, eukaryotes, and archaea residing in the gut is termed the intestinal microbiota, with bacteria constituting its dominant domain. The composition and diversity of this microbiome are vital for host metabolism, protection against pathogens via nutrient competition and immune priming⁵, and the preservation of intestinal epithelial homeostasis. Growing evidence indicates that diabetes is associated with a state of dysbiosis, in which the microbiota shifts toward a pathogenic profile. This imbalance compromises intestinal barrier function, interferes with host signaling pathways, and ultimately drives chronic low-grade inflammation⁶.

Vitamin D is a fat-soluble vitamin with 1,25(OH)₂D₃ as the main active form, which has been proven to regulate cell proliferation, differentiation, apoptosis, and autophagy^{7,8}. Over the past decade, low blood

¹Center of Laboratory Animal, Suzhou Medical College of Soochow University, Suzhou, China. ²CCIC Huatongwei International Inspection(Suzhou)Co.,Ltd, Suzhou, China. ³Center of Laboratory Animal, Shanghai Jiao Tong University, Shanghai, China. ⁴Lewen Zhang and Lijuan Zhao contributed equally to this work. ✉email: clxiao@suda.edu.cn; zacharyzhou@suda.edu.cn

25-hydroxyvitamin D (25(OH)D) levels have been highlighted as a risk factor for T2DM⁹. Vitamin D supplementation has been shown to reduce the risk of diabetes through its anti-inflammatory and anti-fibrotic effects along with vitamin D receptor (VDR). While the interaction between vitamin D and gut microbiota has been well elucidated in the context of gastrointestinal diseases¹⁰, its specific role in T2DM remains to be clarified.

Materials and methods

Mice

Fifty 6-week-old male C57BL/6J mice (20–24 g) were purchased from Beijing Vital River Laboratory Animal Technology Co., Ltd. The mice were housed in the barrier facility of the Experimental Animal Center of Soochow University, with a room temperature of 22 ± 2 °C, relative humidity of $55\% \pm 5\%$, and a 12-h/12-h light/dark cycle (license No. SYXK(Su)2021-0065). All experimental animal procedures conformed to the requirements of the Experimental Animal Ethics Committee of Soochow University and were implemented in accordance with the Guidelines for the Ethical Review of Laboratory Animal Welfare and ARRIVE guidelines.

Establishment of the T2DM mouse model

The mice were fed a high-fat diet (60% from fat, 20% from carbohydrates and 20% from protein, Double lion experimental animal feed technology CO., LTD., Jiangsu, China) for 4 weeks and fasted for 12 h, before intraperitoneally injecting streptozotocin (STZ) (St. Louis, Sigma Aldrich, MO, United States) at a dose of 100 mg/kg. The dose of STZ applied to establish a diabetic in vivo model conformed to the previous studies¹¹. The fasting blood glucose (FBG) of the mice was detected by tail clipping on days 3, 5, and 7, and the blood glucose value reached 16.7 mmol/L for two consecutive measurement times, indicating successful establishment of the T2DM mouse model. The cages of the model mice were replaced regularly to ensure adequate food and drinking water.

Experimental groups

All mice were divided into four groups: Wild type (WT) group, WT-VD group, DM group and DM-VD group. T2DM mouse modeling was performed in DM group and DM-VD group. After successful modeling, conventional diet and water were consumed and mice were intraperitoneally injected with peanut oil or 1,25(OH)₂D₃ (Sigma, St. Louis, MO, USA) at 5 µg/kg every other day. The doses of 1,25(OH)₂D₃ used to treat T2DM were based on previous research¹².

Sample collection

After 4 weeks of 1,25(OH)₂D₃ treatment, blood samples were collected and left at room temperature for 2 h, before moving to 4 °C overnight to allow the blood to coagulate. The next day, serum samples were obtained by centrifugation at low speed. Mouse feces were collected, frozen in liquid nitrogen, and stored at –80 °C. All mice were euthanized by cervical dislocation after death was confirmed via overdose anesthesia with carbon dioxide (CO₂ concentration: 40%). Tissues and organs were immediately collected thereafter. After rinsing pancreatic and colon tissues with phosphate buffered saline (PBS), the required parts were placed in 4% paraformaldehyde, and the rest was stored at –80 °C.

Glucose tolerance

The day before the end of the experiment, the mice in each group were fasted for 12 h, and glucose was administered intragastrically at a dose of 2 g/kg at 0, 0.5, 1, and 2 h to detect the blood glucose values of each phase, before calculating the area under the curve (AUC).

Enzyme-linked immunosorbent assay (ELISA)

The levels of glycated hemoglobin A1c (GHbA1c), insulin (INS), interleukin-1beta (IL-1 β), tumor necrosis factor-alpha (TNF- α), reactive oxygen species (ROS), catalase (CAT), and malondialdehyde (MDA) in the supernatant of each group of cells or mouse serum were detected by ELISA.

Histological observations

For histological analysis, 5-µm sections were obtained from paraffin-embedded samples and subjected to hematoxylin and eosin (HE) staining. The structural changes were visualized by light microscopy (Leica, Wetzlar, Germany), and the ultrastructure of the colon was observed by transmission electron microscopy (TEM) (Hitachi, Tokyo, Japan).

Reverse transcription-quantitative PCR (RT-qPCR)

Quantitative PCR (qPCR) was performed to analyze ZO-1 and Occludin in colon tissue. Total RNA was extracted using RNAisoPlus (TaKaRa, Tokyo, Japan) according to the manufacturer's instructions. Total RNA was reverse-transcribed into cDNA using a reverse transcription kit (Vazyme, Nanjing, China), followed by qPCR with SYBR Green (Vazyme) using a real-time PCR system (Bio-Rad, Hercules, CA, USA). The reaction conditions were as follows: stage 1, 95 °C for 10 s and stage 2, 40 cycles of 95 °C for 10 s and 60 °C for 30 s. GAPDH was used as an internal control. The primer sequences are listed in Table 1.

Western blotting

To extract proteins, colon tissue was collected, washed twice with ice-cold PBS, and solubilized in lysis buffer (RIPA, Beyotime, Beijing, China) supplemented with proteinase inhibitor (PMSF, Beyotime). Subsequently, the sample was homogenized on ice until the tissue mass disappeared and the liquid became clear. The lysates were then centrifuged at 12,000 rpm at 4 °C to remove debris. The protein concentration was determined using a

Gene	Forward primer	Reverse primer
Zonulaoccludens-1 (ZO-1)	AATGCTGCTTATTGGG	AGTGGTGGTGGTCTTCT
Occludin	AAGAGTTGACAGTCCCATGGCATAAC	ATCCACAGGCAGTAAATGGAAG
Glyceraldehyde-3-phosphate dehydrogenase (GAPDH)	CGTCCCGTAGACAAAATGGT	TTGATGGCAACAATCTCCAC

Table 1. Primers used for reverse transcription-quantitative PCR (RT-qPCR) analysis.

BCA kit (Beyotime). Equal quantities of protein were separated using SDS-polyacrylamide gel electrophoresis. After protein quantification and denaturation, SDS-polyacrylamide gel was prepared for electrophoresis. The loading concentration was 5 µg/uL and the loading volume was 10 µL. The constant voltage is 80 V, and when the Marker runs out of the rainbow strip, the voltage is adjusted to 120 V until the bromophenol blue runs to the bottom. The proteins were transferred to a PVDF membrane, which was blocked with 5% skim milk after ice bath. For targeted imaging and optimization of antibody conditions during the study, lanes containing the proteins of interest were excised from the gel prior to electrophoretic transfer. Western blotting was performed using the following primary antibodies: Zonulaoccludens-1 (ZO-1) (1:1000, ABclonal, Wuhan, China), occludin (1:1000, ABclonal), NDUFB8 (1:1000, ABclonal), SIRT1 (1:1000, ABclonal), AMPK (1:1000, ABclonal), and pAMPK (1:1000, ABclonal). After washing, the membranes were incubated with peroxidase-labeled secondary anti bodies (1:10000, Abcam, Cambridge, MA, USA) at 37 °C for 2 h. Immunoreactive bands were detected using ECL (Beyotime), and the chemidoc XRS + imaging system (Bio-Rad) was used to take photomicrographs. The experiments were repeated at least three times.

Immunohistochemistry assays

Immunohistochemical staining was performed for ZO-1 and occludin. Briefly, sections were blocked with 5% bovine serum albumin and then incubated with the primary antibodies, ZO-1 (1:200, ABclonal) and occludin (1:200, ABclonal), overnight at 4 °C. Subsequently, the sections were incubated with the corresponding secondary antibody (Sigma, Saint Louis, MO, USA) at room temperature for 2 h. Finally, the slides were stained with DAB for 30 min, and images were acquired using a light microscopy (Leica). The quantitative data of the above assays were analyzed using ImageJ software.

16SrDNA

Total bacterial DNA was extracted using a DNA isolation kit (GUHE, Hangzhou, China) according to the manufacturer's instructions. The quantity and quality of extracted DNA were measured using a NanoDrop ND-1000 spectrophotometer (Thermo Fisher Scientific, Waltham, MA, USA) and agarose gel electrophoresis, respectively. PCR amplification of the bacterial 16SrRNA gene V4 region was performed using the forward primer 515 F (5'- GTGCCAGCMGCCGCGTAA-3') and reverse primer 806R (5'-GGACTACHVGGGTWTCTAAT-3'). Sequencing of polymerase chain reaction products was performed using the Illumina NovaSeq6000 platform (Illumina, San Diego, CA, USA). Using the Vsearch software platform (v2.4.4), we employed the UNOISE2 algorithm to denoise the sequences, which included removing sequences with lengths below 4 base pairs to generate an OTU feature table. The sample data were then normalized by Total Sum Scaling (TSS) and rarefied to a uniform depth of 100,000 reads per sample, resulting in an ASV table. Following taxonomic annotation, ASVs with an average abundance below 0.01% were filtered out. Subsequent analyses were performed based on this processed ASV table. Trimmed sequences were demultiplexed and quality filtered using Quantitative Insights into Microbial Ecology (QIIME2) and R software (v3.2.0). Downstream analyses, such as Venn diagrams, Shannon index, Principal Coordinate Analysis (PCoA) based on the unweighted Unifrac distance, Linear discriminant analysis Effect Size (LEfSe) and Heatmap of Spearman's correlation analysis, were performed using MicrobiomeAnalyst (v2.0). Statistical Analysis of Metagenomic Profiles (STAMP) v2.0.0 was used to analyze and visualize the changes in the predictive function of intestinal microbiota.

Statistical methods

All data are expressed as the mean ± SD for each group. The data were analyzed by one-way analysis of variance (ANOVA). P-values < 0.05 were considered to indicate statistical significance. GraphPad Prism 9.0 software (GraphPad Software, San Diego, California, USA) and ImageJ (v1.53) (National Institutes of Health, Bethesda, Maryland, USA) were used to perform the statistical analyses.

Results

1,25(OH)₂D₃ improves glucose metabolism in T2DM mice

After HFD/STZ treatment, the blood glucose of the model mice reached 16.7 mmol/L for two consecutive measurement times, indicating successful establishment of the T2DM model. After 4 weeks of intervention, 1,25(OH)₂D₃ decreased the FBG and GHbA1c levels ($p < 0.001$ and $p < 0.0001$), promoted insulin secretion ($p < 0.01$), and improved glucose tolerance ($p < 0.01$) compared to the DM group (Fig. 1).

1,25(OH)₂D₃ inhibits oxidative stress and inflammation in T2DM mice

Consistently high blood glucose levels can contribute to inflammation and oxidative stress. Therefore, we next measured the pancreatic histopathological changes (Fig. 2a) and serum levels of Interleukin-1 beta (IL-1 β) (Fig. 2b), tumor necrosis factor alpha (TNF- α) (Fig. 2c), lipopolysaccharide (LPS) (Fig. 2d), reactive oxygen

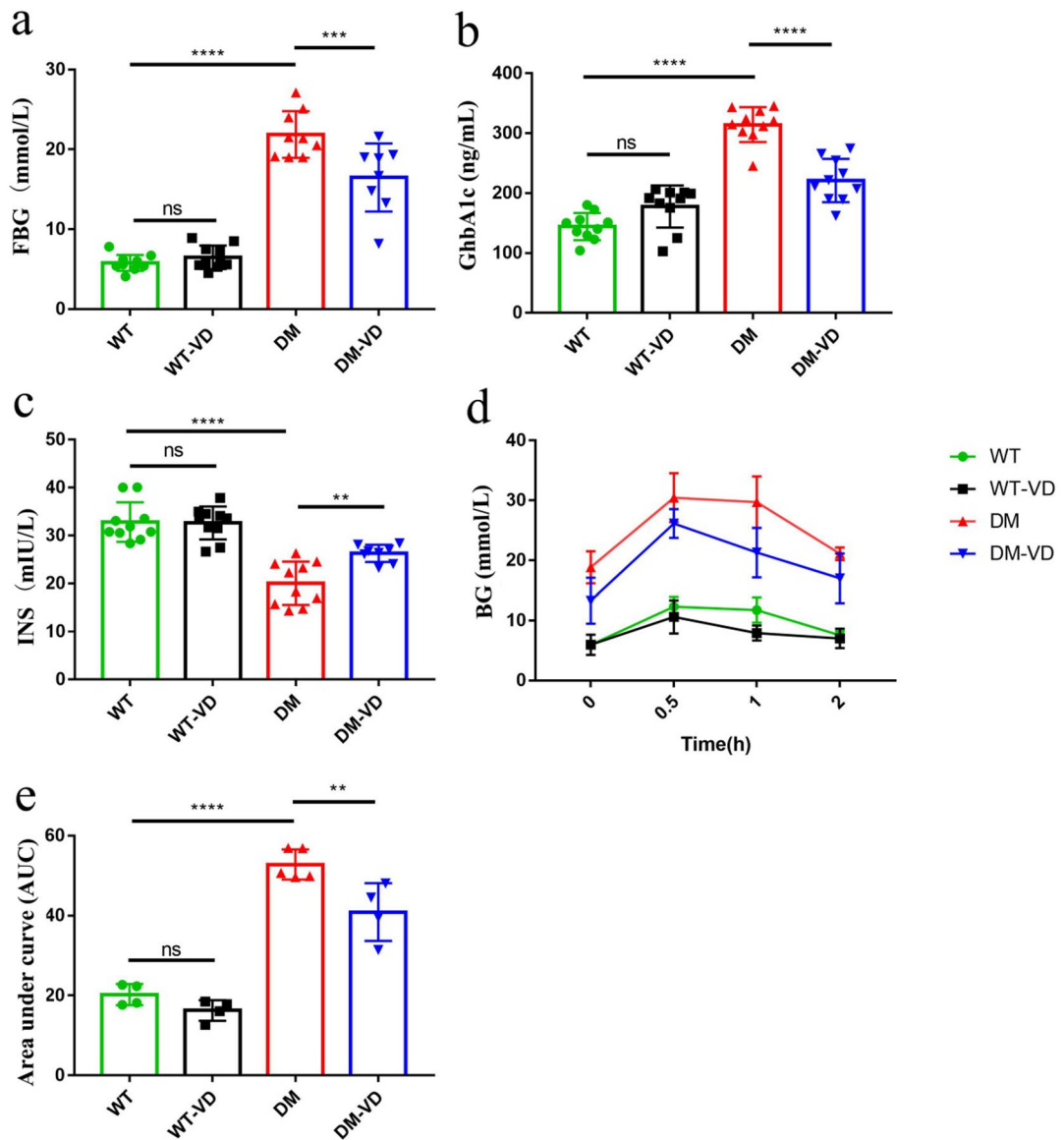


Fig. 1. $1,25(\text{OH})_2\text{D}_3$ reduced blood glucose and improved glucose tolerance. Change in fasting blood glucose (FBG) (a) after 4-week intervention with $1,25(\text{OH})_2\text{D}_3$, (b–c) Quantification of GHbA1c (b) and INS (c) by ELISA after 4-week intervention with $1,25(\text{OH})_2\text{D}_3$, (d–e) Change in the glucose tolerance curve (d) and AUC (e) after 4-week intervention. Each value is expressed as the mean \pm SD. **, ***, and **** indicate significant differences at $p < 0.01$, $p < 0.001$, and $p < 0.0001$, respectively.

species (ROS) (Fig. 2e), malondialdehyde (MDA) (Fig. 2f), catalase (CAT) (Fig. 2g), and total antioxidant capacity (T-AOC) (Fig. 2h) to investigate the production of inflammatory factors and oxidative stress.

The islets of the WT and WT-VD groups exhibited clear boundaries, regular shapes, and uniform cell distributions, whereas those of the DM group were reduced in volume, with unclear boundaries and inflammatory cell infiltration. Compared to the DM group, the volume of islets and the number of cells increased, and inflammatory cell infiltration decreased in the DM-VD group. The ELISA results showed that compared to the WT group, the levels of IL-1 β , TNF- α , LPS, ROS and MDA in the DM group were significantly increased ($p < 0.0001$), whereas the levels of CAT and T-AOC were significantly decreased ($p < 0.0001$), demonstrating the presence of systemic inflammation and excessive oxidative stress. After $1,25(\text{OH})_2\text{D}_3$ intervention, the content of IL-1 β , TNF- α and MDA in the DM-VD group was significantly decreased ($p < 0.01$ and $p < 0.05$), and the LPS and ROS level was slightly decreased ($p > 0.05$).

$1,25(\text{OH})_2\text{D}_3$ affects intestinal microbiota diversity

Next, 16S rDNA amplicon sequencing was used to analyze the effect of $1,25(\text{OH})_2\text{D}_3$ intervention on intestinal microbiota in T2DM mice. The Venn diagram and α and β diversity analysis showed differences in intestinal microbiota diversity among the groups. The OTU diagram showed differences in the microflora of each group, indicating that the subsequent analysis was meaningful (Fig. 3a). The diversity and richness of the gut microbial

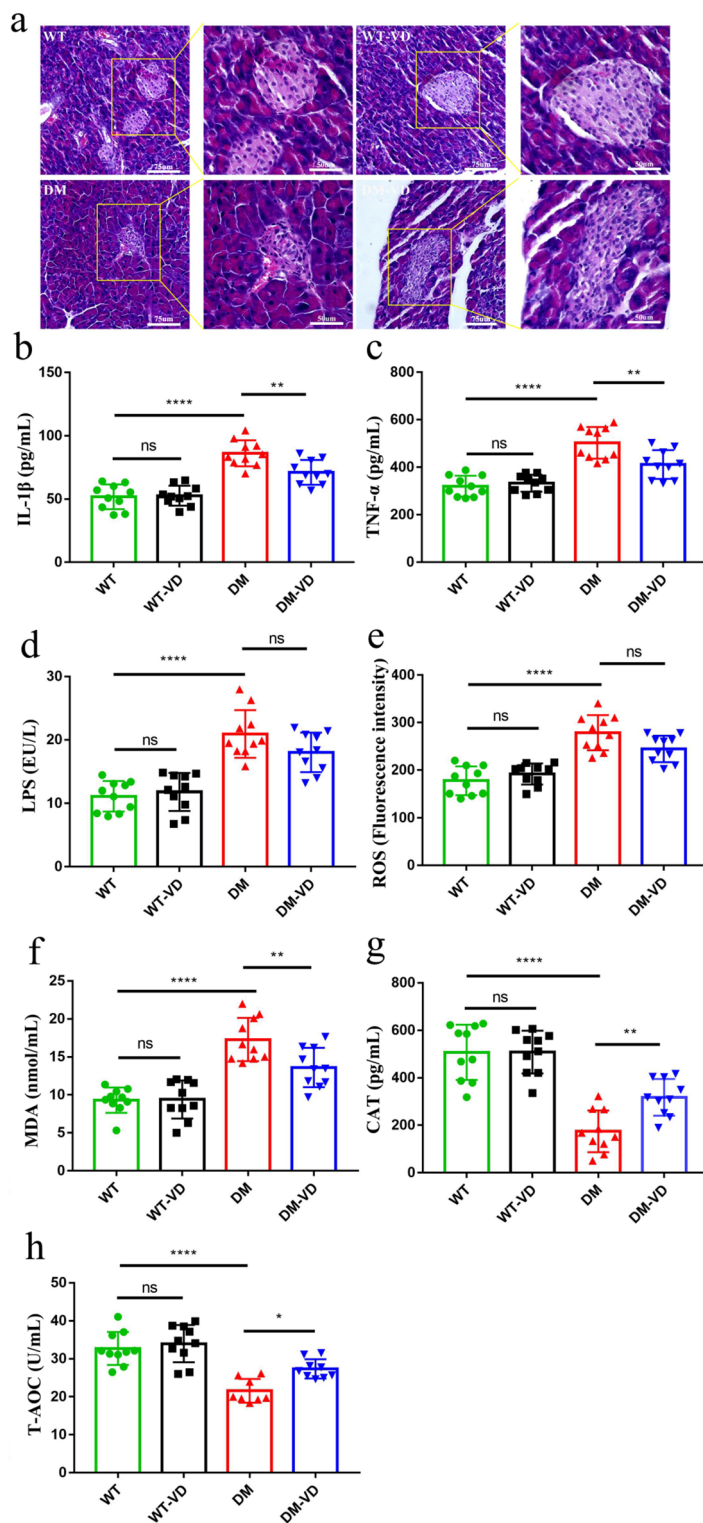


Fig. 2. $1,25(\text{OH})_2\text{D}_3$ played an anti-inflammatory and antioxidant role in T2DM mice. **(a)** Representative images of hematoxylin and eosin staining (HE) of the pancreatic tissue (magnification = $\times 200$, scale bar: 50 μm). The right image is the enlarged image inside the yellow frame in the left image. **(b-h)** Quantification of IL-1 β **(b)**, TNF- α **(c)**, LPS **(d)**, ROS **(e)**, MDA **(f)**, CAT **(g)**, and T-AOC **(h)** in serum after 4-week intervention with $1,25(\text{OH})_2\text{D}_3$. Each value is expressed as the mean \pm SD. *, **, and **** indicate significant differences at $p < 0.05$, $p < 0.01$, and $p < 0.0001$, respectively.

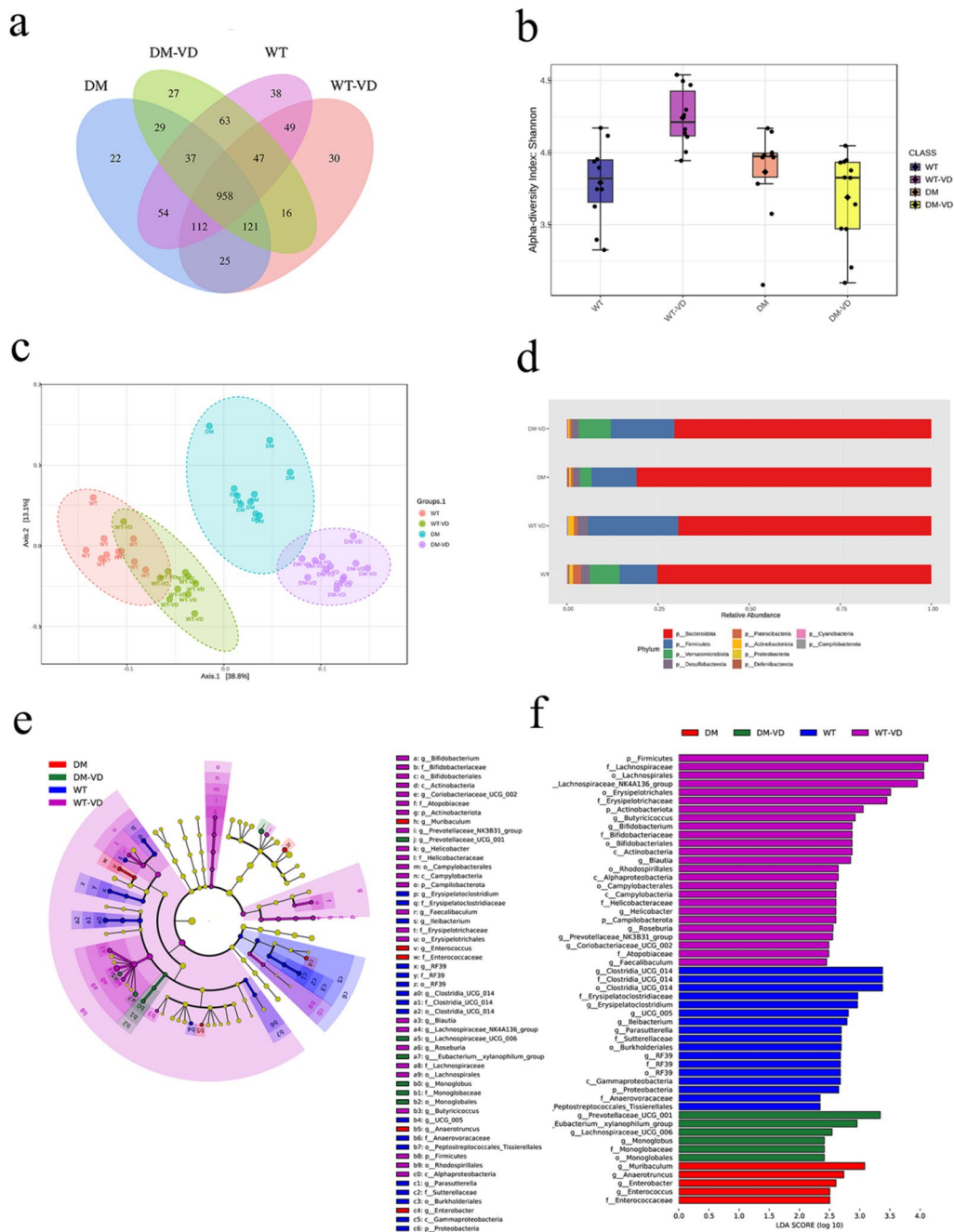


Fig. 3. 1,25(OH)₂D₃ affected the diversity of intestinal microbiota and changed the dominant bacterial genera. Venn diagram (**a**), Shannon index (**b**), Principal Coordinate Analysis (PCoA) based on the unweighted Unifrac distance (**c**), and relative abundance at the phylum level (**d**) of microbiota among groups. Linear discriminant analysis Effect Size (LEfSe) was used to analyze the most differential taxa in the different groups (**e**). The enriched taxa with an LDA score > 2 in each group are shown in different colors (**f**).

composition were evaluated using a diversity analysis. The Shannon index represents species diversity, that is, community composition heterogeneity. Compared to the WT group, the Shannon index of the DM group was slightly higher, indicating that the species diversity increased. Additionally, the DM-VD group exhibited a decrease in the Shannon index compared to the DM group, suggesting that vitamin D has a negative effect on species diversity. However, both the species richness and diversity were higher in the WT-VD group than in the other treatment groups (Fig. 3b). Principal Coordinate Analysis (PCoA) based on the unweighted Unifrac distance showed that the DM and WT groups were completely separated, indicating a significant difference in intestinal microbiota composition, while $1,25(\text{OH})_2\text{D}_3$ intervention also impacted the intestinal microbiota composition of T2DM mice (Fig. 3c).

The intestinal species information was annotated using the SILVA138 database. Compared to the WT group, there were differences in the top 10 most abundant phyla in the DM group, especially *Bacteroidetes* and *Firmicutes*, the two dominant phyla, indicating that the pathological status of T2DM affected the colonization of dominant bacteria. The DM-VD group exhibited reduced *Firmicutes* and enriched *Bacteroidetes* relative to the DM group. The proportion of these two dominant categories in the DM-VD group was more similar to that in the WT group. The *Firmicutes/Bacteroidota* (F/B) ratio is a key indicator of gut microbiota dysbiosis. Additionally, compared to the WT group, the relative abundance of *Verrucomicrobia* was decreased in the DM group. The relative abundance of *Verrucomicrobia* increased in the DM-VD group. However, compared to the WT group, *Verrucomicrobia* showed a tendency to die out in the WT-VD group (Fig. 3d).

Linear discriminant analysis Effect Size (LEfSe) analysis revealed significant differences in species between groups. The evolutionary cladogram showed that the WT-VD group exhibited richer species diversity than the WT group, while the DM group was enriched in *Enterococcus* and *Enterobacter*. Compared to the DM group, the DM-VD group was enriched in *Prevotellaceae_UCG_001* and *Lachnospiraceae_UCG_006*, among others (Fig. 3e). The bar chart more directly shows the different bacterial genera among the groups and is consistent with the results of the evolutionary cladistic chart (Fig. 3f).

1,25(OH)₂D₃ changed the function of the intestinal microbiota

The cluster heatmap showed the differences in species composition and abundance more directly, while Spearman correlation analysis was used to determine the correlation between changes in intestinal microbiota and host phenotype. The heatmaps showed that *Enterobacter* and *Enterococcus* were positively correlated with inflammation (LPS, IL-1 β , TNF- α), oxidative stress levels (ROS, MDA), FBG, and GHbA1c ($p < 0.05$ and $p < 0.01$) and negatively correlated with antioxidant stress level (CAT, T-AOC) and insulin secretion level ($p < 0.05$ and $p < 0.01$). *Lachnospiraceae_UCG_006* was negatively correlated with inflammation (LPS, IL-1 β , TNF- α), oxidative stress levels (ROS, MDA), and blood glucose levels (FBG, GHbA1c) ($p < 0.01$), whereas it was positively correlated with the levels of antioxidant stress (CAT) and insulin secretion ($p < 0.01$) (Fig. 4a). Additionally, analysis of potential bacterial functions showed that 1,25(OH)₂D₃ significantly downregulates stress response pathways (KO 00053, KO 00250, KO 04141) and proinflammatory response pathways (KO 05111) (Fig. 4b), emphasizing the anti-inflammatory and antioxidant effects of 1,25(OH)₂D₃.

1,25(OH)₂D₃ maintained the integrity of the colonic epithelial barrier

The colon structure consists of four layers, including the mucosal layer, submucosal layer, muscularis propria, and serosal layer, which in turn includes the mucosal epithelium, mucosal lamina propria, and mucosal microvilli. The histological results demonstrated that the intestinal epithelium in the DM group exhibited typical pathological signs, such as partial separation and loss of epithelial cells, deep recesses, and irregular surfaces, accompanied by inflammatory cell infiltration. However, 1,25(OH)₂D₃ intervention normalized the epithelial and mucosal structures and left the glands intact (Fig. 5a).

Tight junction proteins are important for maintaining the integrity of the intestinal barrier. However, compared to the WT group, the expression of ZO-1 and occludin decreased significantly in the DM group ($p < 0.01$ and $p < 0.001$), both of which were significantly upregulated by vitamin D intervention ($p < 0.05$ and $p < 0.01$) (Fig. 5b–j).

Next, the MDA content and SOD enzyme activity were measured to investigate the intestinal redox environment. Compared to the WT group, the MDA content in the DM group was significantly increased ($p < 0.01$), and SOD activity was significantly decreased ($p < 0.0001$). However, compared to the DM group, 1,25(OH)₂D₃ decreased the MDA content ($p < 0.05$), significantly increased SOD activity ($p < 0.001$) (Fig. 5k–l), and improved intestinal oxidative stress.

1,25(OH)₂D₃ activates AMPK signaling and protects mitochondrial function

The TEM results revealed that microvilli were partially absent on the surface of the intestinal epithelium, while the mitochondria varied in shape and size, appeared swollen or even ruptured, and the tight junctions were damaged. In the DM-VD group, the intestinal epithelial microvilli were arranged in a more orderly manner, and the mitochondrial morphology was relieved, although slight swelling remained (Fig. 6a). The loss of NDUFB8 expression also demonstrated the impairment of mitochondrial function in the T2DM group, and the phosphorylation levels of AMPK and SIRT1 were significantly decreased ($p < 0.01$ and $p < 0.0001$). Interestingly, 1,25(OH)₂D₃ promoted NDUFB8 expression and increased pAMPK levels ($p < 0.05$) (Fig. 6b–f). However, the increase in SIRT1 in the DM-VD group was not significant ($p > 0.05$).

Discussion

As a key pathological driver in diabetes, chronic hyperglycemia is responsible for widespread tissue and organ damage, thereby rendering its management a critical objective in T2DM care¹³. In the present investigation, we employed a protocol involving an HFD and a low-dose STZ injection to induce T2DM in mice. This approach effectively produced an animal model that recapitulated major clinical manifestations of the human condition, most notably hyperglycemia and insulin resistance.

Persistent hyperglycemia promotes the non-enzymatic glycation of proteins and lipids, leading to the formation of advanced glycation end products (AGEs). These compounds can induce oxidative stress and tissue damage. Furthermore, AGE accumulation upregulates the expression of the AGE receptor (RAGE), consequently activating inflammatory pathways¹⁴. Consistent with this mechanism, our T2DM model mice exhibited elevated blood glucose, increased oxidative stress, and heightened systemic levels of inflammatory cytokines. These responses exacerbated islet inflammation and cellular injury, thereby increasing the overall inflammatory burden. Epidemiological studies have established a link between T2DM progression and reduced

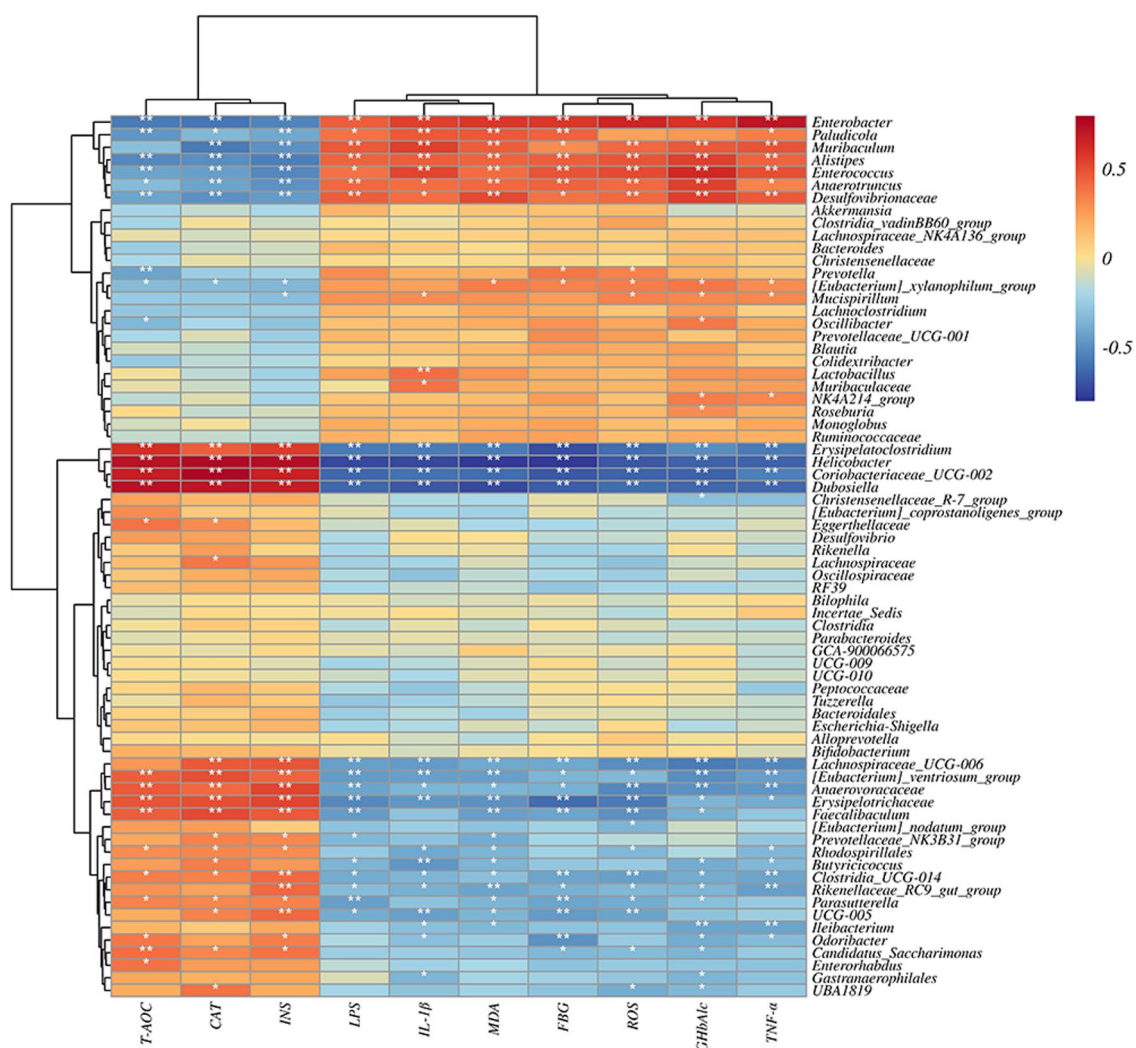
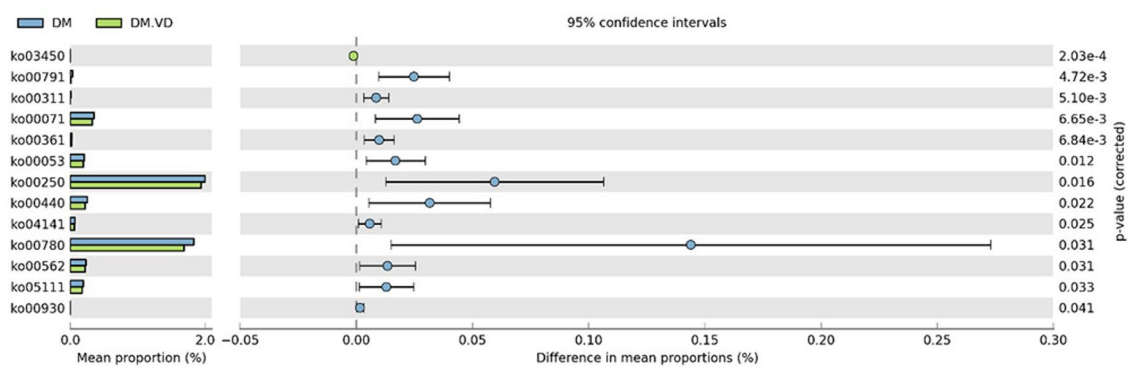
a**b**

Fig. 4. 1,25(OH)₂D₃ downregulated bacteria associated with inflammation and stress pathways. Heatmap of Spearman's correlation analysis between metabolic-related parameters and bacteria at the genus level (a). The correlation between microbial species and biomarkers was visualized by color depth, where the darker the color, the stronger the correlation. Red represents a positive correlation, and blue represents a negative correlation. STAMP was used to analyze and visualize the changes in the predictive function of intestinal microbiota in T2DM and DM-VD mice (b). * and ** indicate significant differences at $p < 0.05$ and $p < 0.01$, respectively.

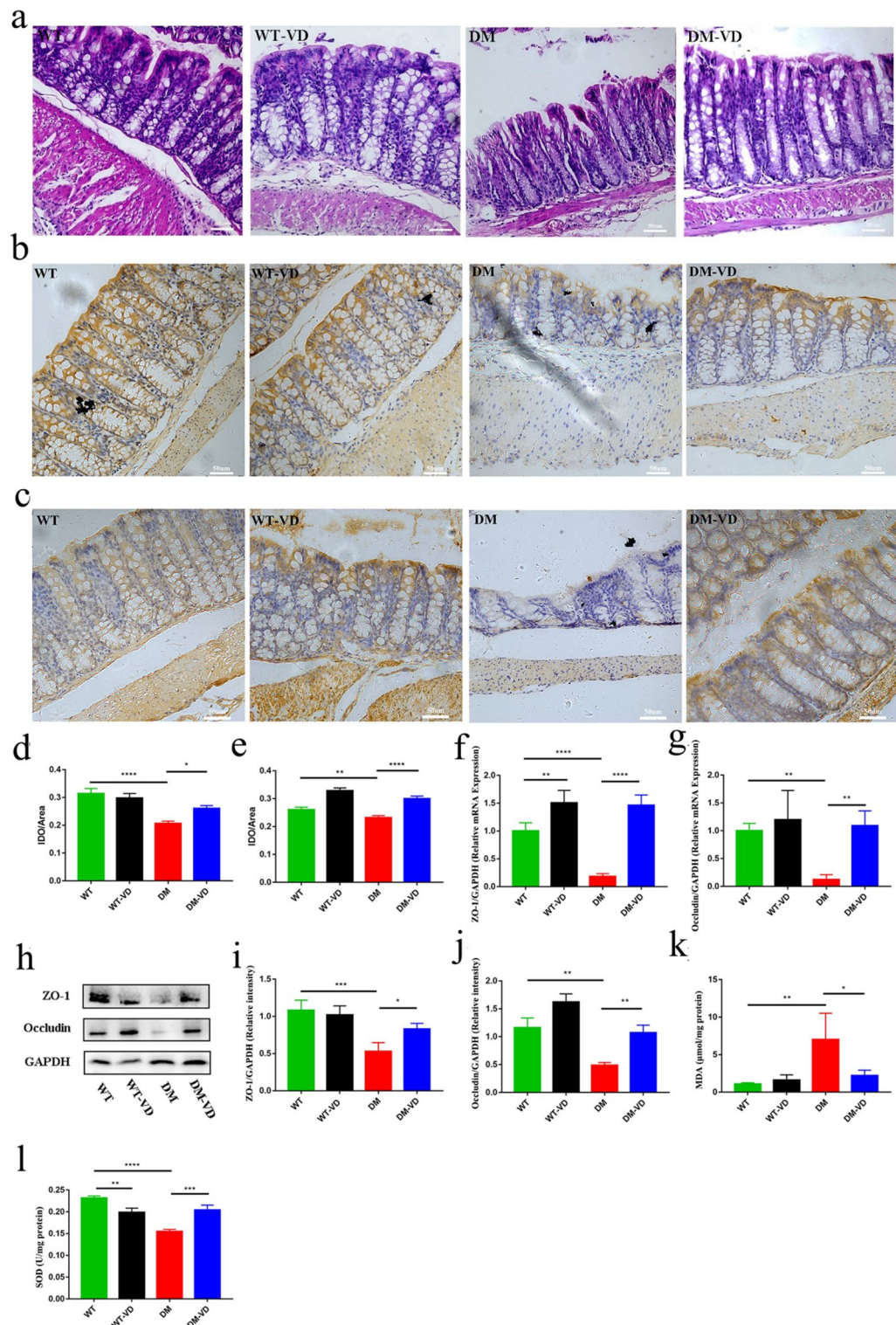


Fig. 5. $1,25(\text{OH})_2\text{D}_3$ improved oxidative stress and alleviated intestinal epithelial injury. **(a)** Representative images of hematoxylin and eosin staining of colon tissue (magnification = $\times 200$, scale bar: 50 μm). Immunohistochemical staining and quantification of ZO-1 **(b)** and occludin **(c)** (magnification scale bar: 50 μm). **(d–e)** IOD value of ZO-1 **(d)** and occludin **(e)**. **(f–g)** Expression of colonic ZO-1 **(f)** and occludin **(g)** mRNA in each group. The results of RNA expression were normalized for glyceraldehyde 3-phosphate dehydrogenase (GAPDH). **(h–j)** Expression levels of ZO-1 and occludin. Quantification of western blot data. **(k–l)** Change in MDA content **(k)** and SOD activity **(l)** in the colon of each group. Each value is expressed as the mean \pm SD. *, **, ***, and **** indicate significant difference at $p < 0.05$, $p < 0.01$, $p < 0.001$, and $p < 0.0001$, respectively.

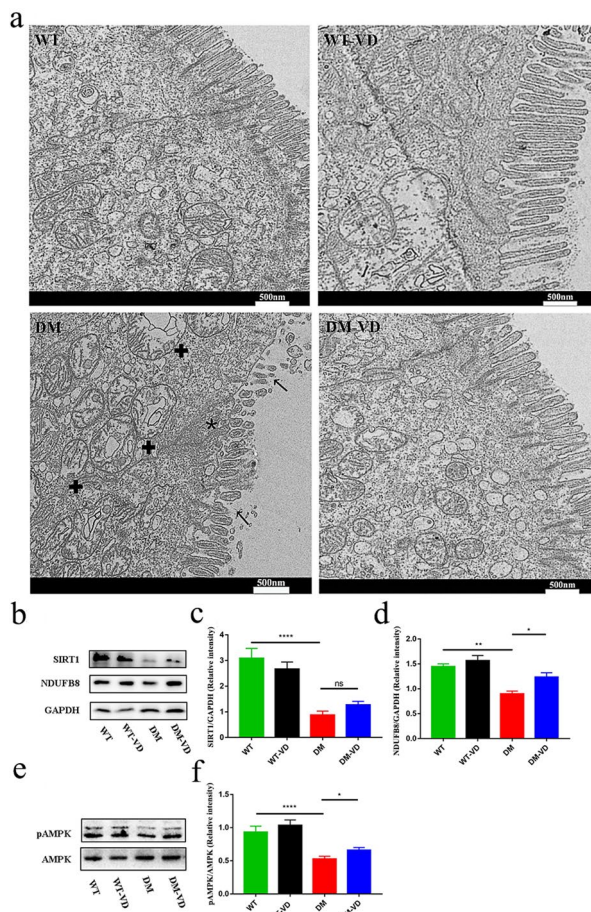


Fig. 6. $1,25(\text{OH})_2\text{D}_3$ protected mitochondrial function and promoted AMPK phosphorylation. **(a)** Representative TEM images of the colon; magnification = $\times 6000$, scale bar: 500 nm; \blacktriangleleft : Swollen mitochondria; \nwarrow : Shortened microvilli; \star : Damaged tight connection. **(b-d)** Expression levels of SIRT1 and NDUFB8. Quantification of western blot data. **(e-f)** Expression and quantification of phosphorylated AMPK. Each value is expressed as the mean \pm SD. *, **, and **** indicate significant differences at $p < 0.05$, $p < 0.01$, and $p < 0.0001$, respectively.

circulating $25(\text{OH})\text{D}$ levels, noting that the seasonal aggravation of T2DM in winter often coincides with a higher prevalence of vitamin D deficiency^{3,15}. This evidence underscores the relevance of vitamin D supplementation. In our study, compared with the T2DM group, the DM-VD group demonstrated significantly lower blood glucose, reduced oxidative stress, diminished inflammatory cytokines, and attenuated islet damage, confirming the beneficial role of vitamin D.

T2DM is the result of complex gene-environment interactions¹⁶, in which the intestinal microbiota have been shown to play a role. As a harmful metabolite of the intestinal microbiota, LPS circulates at increased levels in the blood of T2DM mice, where it is recognized by the immune system, resulting in the initiation of the inflammatory response. In contrast, the amount of LPS is reduced in the DM-VD group. On the basis of 16S rRNA sequencing, differences in the composition and structure of intestinal microbiota were detected. The result of a diversity analysis showed that the intestinal microbiota diversity was increased in the T2DM group compared to that in the WT group; however, this trend was reversed in DM-VD mice for reasons that remain unclear. Moreover, the Venn diagram confirmed the differences in the intestinal microbiota of mice in each treatment group, indicating the possibility that the intestinal microbiota participate in disease lesions. The results of β diversity analysis further demonstrated the correlation between the pathological status of T2DM and the structural composition of intestinal microbiota. However, the finding that the structural composition of the intestinal microbiota was changed indicates that intestinal physiology is also affected in the pathological state of T2DM.

Bacteroidetes and *Firmicutes* are the two predominant categories in the distal gut microbiota. The relative abundance of these two dominant bacteria in T2DM model mice was affected by systemic inflammatory status, while *Enterococcus* and *Enterobacter* were enriched. *Enterococcus* and *Enterobacter* are facultative anaerobic bacteria, often considered as conditioned pathogens, which promote bacterial translocation and initiate inflammatory responses¹⁷⁻²⁰. Additionally, the relative abundance of *Verrucomicrobia* was also reduced in the microflora of T2DM mice. *Akkermansia muciniphila* is the leading representative and often considered to be

good for health²¹. Cluster heatmap analysis showed that these bacteria were involved in oxidative stress and inflammation and were closely related to blood sugar levels. Intervention with 1,25(OH)₂D₃ reversed this phenomenon and enriched *Lachnospiraceae_UCG_006* as well as others responsible for regulating metabolic disorders. To investigate the causes of these changes in bacteria, we predicted the function of the intestinal microbiota by KEGG analysis. Compared to the DM group, the stress response and pro-inflammatory response pathways were significantly downregulated in the DM-VD group, emphasizing the improvement of the intestinal environment by 1,25(OH)₂D₃, which may be related to anti-inflammatory and anti-stress effects.

An intact intestinal barrier is essential for maintaining a healthy gut microenvironment and a stable microbial community²². In T2DM mice, the intestinal epithelium exhibited marked oxidative stress and injury, accompanied by a significant downregulation of tight junction proteins. ZO-1 and occludin, two key proteins critical to epithelial integrity, are known to be suppressed by pro-inflammatory cytokines such as IL-1 β and TNF- α , which act in part through the MLCK signaling pathway²³. Intestinal epithelial injury can increase intestinal oxygen partial pressure, promote oxidative stress, and further damage the intestinal barrier. As a result, the intestinal microbiota transform into a proinflammatory state and generate several conditioned bacteria, such as *Enterococcus* and *Enterobacter*^{24,25}. MDA is a key mediator that causes intestinal epithelial cell death and intestinal barrier damage, and it mediates apoptosis by inducing mitochondrial damage²⁶. However, the SOD enzyme can effectively remove free radicals and reduce tissue oxidative stress damage. Our results revealed that the MDA content in the colon tissue of T2DM mice increased significantly, whereas the SOD activity decreased. These findings indicate that T2DM creates a deleterious intestinal environment that favors the proliferation of facultative anaerobic pathogens, which in turn sustain epithelial stimulation and perpetuate a cycle of gut dysfunction.

Mitochondria are important mediators that ensure the energy supply of the intestinal epithelium and maintain the anaerobic environment of the intestinal cavity²⁷. In the pathological T2DM state, the mitochondria were swollen, some ridges were missing, and the expression of mitochondrial complex I subunit NDUF8 was significantly downregulated, which disrupted energy production. Treatment with 1,25(OH)₂D₃ promoted NDUF8 expression, improved mitochondrial morphology and function, and protected the intestinal epithelium from oxidative stress damage, which may be associated with the integrity of the intestinal epithelial barrier. Our results also demonstrated downregulation of AMPK phosphorylation and its downstream regulatory protein SIRT1, indicating that the AMPK/SIRT1 signaling pathway was inhibited in the intestinal tissue of T2DM mice. The AMPK signaling pathway is critical for sensing energy demand and cellular stress and represents an important target for the anti-inflammatory and autophagic effects of 1,25(OH)₂D₃^{28,29}. However, the relationship between 1,25(OH)₂D₃ and the AMPK signaling pathway in the intestinal tissue remains unclear. While 1,25(OH)₂D₃ significantly enhanced AMPK phosphorylation in T2DM mice, its impact on SIRT1 was not statistically significant, implying the involvement of alternative pathways in barrier protection. Studies have shown that nuclear factor-erythroid 2-related factor 2 (Nrf2) and SOD can be unregulated by vitamin D signals to inhibit oxidative stress, and promote mitochondrial renewal, thereby improving the dysregulated redox state and helping to maintain intestinal health³⁰.

Conclusion

Vitamin D, a pleiotropic secosteroid hormone, exhibits protective associations with T2DM pathogenesis through unresolved mechanisms. This study elucidates that 1,25(OH)₂D₃ administration induced compositional remodeling of intestinal microbiota, characterized by reduced abundance of proinflammatory bacterial taxa and enrichment of commensal species with metabolic stabilizing potential. These coordinated adaptations correlated with glycemic control, oxidative stress and inflammatory response. Notably, 1,25(OH)₂D₃ enhances AMPK phosphorylation in colonic tissues, a regulatory node associated with improved intestinal epithelial integrity and mitochondrial bioenergetics, suggesting vitamin D-AMPK axis modulation may be an effective strategy to ameliorate microbiota-metabolism crosstalk in T2DM. Our findings provide mechanistic evidence linking vitamin D-mediated intestinal microenvironment stabilization to its anti-diabetic effects, advancing understanding of nutritional interventions in metabolic disorders.

Data availability

All data generated or analysed during this study are included in this published article (and its Supplementary Information files).

Received: 10 July 2025; Accepted: 6 November 2025

Published online: 11 December 2025

References

1. Tomic, D., Shaw, J. E. & Magliano, D. J. The burden and risks of emerging complications of diabetes mellitus. *Nat. Rev. Endocrinol.* **18**, 525–539 (2022).
2. Maphumulo, S. C. & Pretorius, E. Role of Circulating microparticles in type 2 diabetes mellitus: implications for pathological clotting. *Semin Thromb. Hemost.* **48**, 188–205 (2022).
3. Wu, Y., Ding, Y., Tanaka, Y. & Zhang, W. Risk factors contributing to type 2 diabetes and recent advances in the treatment and prevention. *Int. J. Med. Sci.* **11**, 1185–1200 (2014).
4. Musso, G., Gambino, R. & Cassader, M. Interactions between gut microbiota and host metabolism predisposing to obesity and diabetes. *Annu. Rev. Med.* **62**, 361–380 (2011).
5. Xu, W. T., Nie, Y. Z., Yang, Z. & Lu, N. H. The crosstalk between gut microbiota and obesity and related metabolic disorders. *Future Microbiol.* **11**, 825–836 (2016).
6. Sharma, S. & Tripathi, P. Gut Microbiome and type 2 diabetes: where we are and where to go? *J. Nutr. Biochem.* **63**, 101–108 (2019).

7. de Albuquerque Borborema, M. E., Oliveira, D. C. & de Azevêdo Silva, J. Down regulation of VDR gene expression in metabolic syndrome and atherosclerosis' patients: cause or consequence? *Gene* **771**, 145341 (2021).
8. Zheng, M., Gao, R. & Vitamin, D. A potential star for treating chronic pancreatitis. *Front. Pharmacol.* **13**, 902639 (2022).
9. Pittas, A. G., Jorde, R., Kawahara, T. & Dawson-Hughes, B. Vitamin D supplementation for prevention of type 2 diabetes mellitus: to D or not to D? *J. Clin. Endocrinol. Metab.* **105**, 3721–3733 (2020).
10. Shang, M., Sun, J. & Vitamin, D. V. D. Probiotics, and Gastrointestinal diseases. *Curr. Med. Chem.* **24**, 876–887 (2017).
11. Lee, H. & Lim, Y. Tocotrienol-rich fraction supplementation reduces hyperglycemia-induced skeletal muscle damage through regulation of insulin signaling and oxidative stress in type 2 diabetic mice. *J. Nutr. Biochem.* **57**, 77–85 (2018).
12. Wang, Y. et al. Vitamin D induces autophagy of pancreatic β -cells and enhances insulin secretion. *Mol. Med. Rep.* **14**, 2644–2650 (2016).
13. Park, J. E., Son, J., Seo, Y. & Han, J. S. HM-Chromanone ameliorates hyperglycemia and dyslipidemia in type 2 diabetic mice. *Nutrients* **14** (2022).
14. Lee, J., Yun, J. S. & Ko, S. H. Advanced glycation end products and their effect on vascular complications in type 2 diabetes mellitus. *Nutrients* **14** (2022).
15. Zhang, Y. et al. Effects of vitamin D supplementation on prevention of type 2 diabetes in patients with prediabetes: A systematic review and Meta-analysis. *Diabetes Care.* **43**, 1650–1658 (2020).
16. Karlsson, F. H. et al. Gut metagenome in European women with normal, impaired and diabetic glucose control. *Nature* **498**, 99–103 (2013).
17. García-Solache, M. & Rice, L. B. The enterococcus: a model of adaptability to its environment. *Clin Microbiol. Rev* **32** (2019).
18. Yang, Y. et al. Within-host evolution of a gut pathobiont facilitates liver translocation. *Nature* **607**, 563–570 (2022).
19. Davin-Regli, A., Lavigne, J. P. & Pages, J. M. Enterobacter spp.: update on Taxonomy, clinical Aspects, and emerging antimicrobial resistance. *Clin Microbiol. Rev* **32** (2019).
20. Si, J. et al. Gut Microbiome signatures distinguish type 2 diabetes mellitus from non-alcoholic fatty liver disease. *Comput. Struct. Biotechnol. J.* **19**, 5920–5930 (2021).
21. Dao, M. C. et al. Akkermansia muciniphila and improved metabolic health during a dietary intervention in obesity: relationship with gut Microbiome richness and ecology. *Gut* **65**, 426–436 (2016).
22. Usuda, H., Okamoto, T. & Wada, K. Leaky gut: effect of dietary fiber and fats on Microbiome and intestinal barrier. *Int J. Mol. Sci* **22** (2021).
23. Shen, L. Tight junctions on the move: molecular mechanisms for epithelial barrier regulation. *Ann. N Y Acad. Sci.* **1258**, 9–18 (2012).
24. Thaiss, C. A. et al. Hyperglycemia drives intestinal barrier dysfunction and risk for enteric infection. *Science* **359**, 1376–1383 (2018).
25. Allam-Ndoul, B., Castonguay-Paradis, S. & Veilleux, A. Gut microbiota and intestinal trans-epithelial permeability. *Int J. Mol. Sci* **21** (2020).
26. Qi, X. et al. Mechanism and intervention measures of iron side effects on the intestine. *Crit. Rev. Food Sci. Nutr.* **60**, 2113–2125 (2020).
27. Pinti, M. V. et al. Mitochondrial dysfunction in type 2 diabetes mellitus: an organ-based analysis. *Am. J. Physiol. Endocrinol. Metab.* **316**, E268–e285 (2019).
28. Wu, S., Zou, M. H. & AMPK Mitochondrial Function, and cardiovascular disease. *Int J. Mol. Sci* **21** (2020).
29. Li, A. et al. Vitamin D-VDR (vitamin D receptor) regulates defective autophagy in renal tubular epithelial cell in streptozotocin-induced diabetic mice via the AMPK pathway. *Autophagy* **18**, 877–890 (2022).
30. Sosa-Díaz, E., Hernández-Cruz, E. Y. & Pedraza-Chaverri, J. The role of vitamin D on redox regulation and cellular senescence. *Free Radic Biol. Med.* **193**, 253–273 (2022).

Author contributions

All authors have participated in formulating the hypothesis, executing the work, analyzing the data, writing of the manuscript and have approved the final version for submission. Conceptualization, Zhengyu Zhou, Chunlan Xiao; Data curation, Lewen Zhang; Formal analysis, Lewen Zhang; Lijuan Zhao; Funding acquisition, Zhengyu Zhou; Investigation, Lijuan Zhao, Lewen Zhang, Xun Wei and Yuxuan Zheng; Methodology, Lewen Zhang, Xun Wei and Zhengyu Zhou; Project administration, Zhengyu Zhou; Resources, Lewen Zhang, Yudie Hu, Zhengyu Zhou and Lijuan Zhao; Software, Lewen Zhang, Yuxuan Zheng; Supervision, Lijuan Zhao, Zhengyu Zhou; Validation, Lewen Zhang, Yudie Hu and Yuxuan Zheng; Visualization, Lewen Zhang, Yudie Hu; Writing – original draft, Lewen Zhang, Yudie Hu, Min Xiao and Lijuan Zhao; Writing – review & editing, Lewen Zhang, Yudie Hu, Min Xiao, Lijuan Zhao, Chunlan Xiao and Zhengyu Zhou. All authors read and approved the final manuscript.

Funding

From the National Natural Science Foundation of China (grant numbers 31970505) is gratefully acknowledged.

Declarations

Competing interests

The authors declare no competing interests.

Additional information

Supplementary Information The online version contains supplementary material available at <https://doi.org/10.1038/s41598-025-27937-3>.

Correspondence and requests for materials should be addressed to C.X. or Z.Z.

Reprints and permissions information is available at www.nature.com/reprints.

Publisher's note Springer Nature remains neutral with regard to jurisdictional claims in published maps and institutional affiliations.

Open Access This article is licensed under a Creative Commons Attribution-NonCommercial-NoDerivatives 4.0 International License, which permits any non-commercial use, sharing, distribution and reproduction in any medium or format, as long as you give appropriate credit to the original author(s) and the source, provide a link to the Creative Commons licence, and indicate if you modified the licensed material. You do not have permission under this licence to share adapted material derived from this article or parts of it. The images or other third party material in this article are included in the article's Creative Commons licence, unless indicated otherwise in a credit line to the material. If material is not included in the article's Creative Commons licence and your intended use is not permitted by statutory regulation or exceeds the permitted use, you will need to obtain permission directly from the copyright holder. To view a copy of this licence, visit <http://creativecommons.org/licenses/by-nc-nd/4.0/>.

© The Author(s) 2025